Research Article

Belgin Sever, Mehlika Dilek Altıntop*, Yeliz Demir, Cüneyt Türkeş, Kaan Özbaş, Gülşen Akalın Çiftçi, Şükrü Beydemir*, Ahmet Özdemir

A new series of 2,4-thiazolidinediones endowed with potent aldose reductase inhibitory activity

https://doi.org/10.1515/chem-2021-0032
received December 2, 2020; accepted February 9, 2021

Abstract: In an effort to identify potent aldose reductase (AR) inhibitors, 5-(arylidene)thiazolidine-2,4-diones (**1**–**8**), which were prepared by the solvent-free reaction of 2,4-thiazolidinedione with aromatic aldehydes in the presence of urea, were examined for their *in vitro* AR inhibitory activities and cytotoxicity. 5-(2-Hydroxy-3-methylbenzylidene)thiazolidine-2,4-dione (**3**) was the most potent AR inhibitor in this series, exerting uncompetitive inhibition with a K_i value of 0.445 ± 0.013 μM. The IC_{50} value of compound **3** for L929 mouse fibroblast cells was determined as 8.9 ± 0.66 μM, pointing out its safety as an AR inhibitor. Molecular docking studies suggested that compound **3** exhibited good affinity to the binding site of AR (PDB ID: 4JIR). Based upon *in silico* absorption, distribution, metabolism, and excretion data, the compound is predicted to have favorable pharmacokinetic features. Taking into account the *in silico* and *in vitro* data, compound **3** stands out as a potential orally bioavailable AR inhibitor for the management of diabetic complications as well as nondiabetic diseases.

Keywords: aldose reductase, thiazolidinedione, cytotoxicity, molecular docking

*** Corresponding author: Mehlika Dilek Altıntop,** Department of Pharmaceutical Chemistry, Faculty of Pharmacy, Anadolu University, 26470 Eskişehir, Turkey, e-mail: mdaltintop@anadolu.edu.tr
*** Corresponding author: Şükrü Beydemir,** Department of Biochemistry, Faculty of Pharmacy, Anadolu University, 26470 Eskişehir, Turkey; The Rectorate of Bilecik Şeyh Edebali University, 11230 Bilecik, Turkey, e-mail: sukrubeydemir@anadolu.edu.tr
Belgin Sever, Kaan Özbaş, Ahmet Özdemir: Department of Pharmaceutical Chemistry, Faculty of Pharmacy, Anadolu University, 26470 Eskişehir, Turkey
Yeliz Demir: Department of Pharmacy Services, Nihat Delibalta Göle Vocational High School, Ardahan University, 75700 Ardahan, Turkey
Cüneyt Türkeş: Department of Biochemistry, Faculty of Pharmacy, Erzincan Binali Yıldırım University, 24100 Erzincan, Turkey
Gülşen Akalın Çiftçi: Department of Biochemistry, Faculty of Pharmacy, Anadolu University, 26470 Eskişehir, Turkey

1 Introduction

Type 2 diabetes (T2D) is a chronic life-threatening disease characterized by abnormally high blood glucose levels resulting from impaired response of target tissues to insulin (insulin resistance) and/or progressively reduced function of pancreatic β cells. The global burden of T2D is increasing considerably, and therefore there is an urgent need to develop safe and potent antidiabetic agents [1–5].

Polyol pathway is a two-step metabolic pathway in which glucose is reduced to sorbitol, which is then converted to fructose. The abnormally activated polyol pathway has been reported to participate in the pathogenesis of T2D complications [5–11].

Aldose reductase (AR) catalyzes the NADPH-dependent reduction of glucose to sorbitol as the first and rate-limiting enzyme of the polyol pathway. Under euglycemic conditions, the reduction of glucose is a minor function of AR owing to the relatively low affinity (high K_m) of AR for this substrate. However, under hyperglycemic conditions, excess intracellular glucose leads to an increase in the enzymatic conversion of glucose to sorbitol, NADPH-consuming reaction in tissues possessing insulin-independent glucose transport. Sorbitol does not diffuse readily through cell membranes due to its strong hydrophilic feature and accumulates in cells causing osmotic stress and cellular damage, particularly in lenses. Furthermore, the concurrent NADPH deprivation impairs the activity of other NADPH-dependent enzymes and causes an imbalance between the generation of intracellular reactive oxygen species and cellular antioxidant defense. Concomitantly, pseudohypoxia, which results from the NAD^+ depletion during the oxidation of sorbitol to fructose by sorbitol dehydrogenase, causes further metabolic and signaling alterations by exacerbating redox imbalance. Fructose, the end product of the polyol pathway, is more reactive than glucose as a glycating agent; and the increased formation of fructose also gives rise to pathological conditions by promoting protein glycation and the formation of advanced glycation end products

and thus leading to alterations in protein functions. Apart from its role in T2D complications, AR is an important mediator in oxidative and inflammatory-signaling pathways implicated in the pathophysiology of cardiovascular disorders, sepsis, and cancer. In this context, AR is identified as a multidisease target for the design of potent agents able to counteract the development of long-term T2D complications as well as nondiabetic diseases [5–13].

The recent findings related to the pathophysiological role of AR have led to the discovery of a great variety of AR inhibitors so far, and most of them have been evaluated in preclinical and clinical trials. However, their development is mostly hampered by low *in vivo* potency, adverse effects, or pharmacokinetic drawbacks [5–13].

2,4-Thiazolidinedione (TZD) stands out as a privileged scaffold for the identification of promising therapeutic agents for the management of T2D, targeting a plethora of crucial enzymes/receptors such as peroxisome proliferator-activated receptor gamma, AR, protein tyrosine phosphatase 1B, and so on [14–26]. In the search for novel AR inhibitors, 2,4-TZDs are of great importance as safer bioisosteres of hydantoin, which is considered as the main cause of hypersensitivity reactions provoked by some AR inhibitors, such as sorbinil. Currently, only epalrestat (EPR) bearing a 2-thioxo-4-thiazolidinone scaffold (Figure 1) is commercially available in few Asian countries (such as Japan and India) as an AR inhibitor approved for the management of diabetic neuropathy. This agent is able to slow the progression of diabetic neuropathy and ameliorate its symptoms without any serious side effects after long-term use. However, further long-term comparative studies should be carried out to elucidate its efficacy in different patient populations [5].

Taking into account the knowledge obtained so far [5–26] and the potential of TZD-based small molecules as AR inhibitors [14–26], herein we reported the preparation of new 2,4-TZDs and *in vitro* studies related to their AR inhibitory activities and cytotoxicity toward L929 mouse fibroblast cell line. In an effort to explore their possible binding modes in the binding site of AR, molecular docking studies were performed. *In silico* absorption, distribution, metabolism, and excretion (ADME) studies were also carried out to estimate their physicochemical parameters for the evaluation of their oral bioavailability and drug likeness.

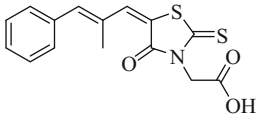

Figure 1: Epalrestat.

2 Experimental section

2.1 Chemistry

2.1.1 General

2,4-TZD and urea were procured from Acros Organics (Geel, Belgium) and VWR Chemicals (Leuven, Belgium), respectively. Aromatic aldehydes were purchased from Alfa Aesar (Karlsruhe, Germany) or Sigma-Aldrich (St. Louis, MO, USA). Melting points (MPs) were detected using Electrothermal IA9200 MP apparatus (Staffordshire, UK). Infrared (IR), nuclear magnetic resonance (NMR; ^{1}H and ^{13}C), mass spectra, and elemental analyses were recorded on IRPrestige-21 FT-IR spectrophotometer (Shimadzu, Tokyo, Japan), Varian 400 MHz FT-NMR spectrometer (Agilent, Palo Alto, CA, USA), VG Quattro Mass spectrometer (Agilent, Minnesota, USA), and Perkin Elmer EAL 240 elemental analyzer (Perkin-Elmer, Norwalk, CT, USA), respectively.

2.1.2 Synthesis of 5-(arylidene)thiazolidine-2,4-diones (1–8)

A mixture of aromatic aldehyde (2 mmol) and 2,4-TZD (2 mmol) in the presence of urea (20 mmol) was heated in an oil bath at 150°C for 2 h. Upon completion of the reaction, it was then dispersed with hot water and collected by filtration. The product was crystallized from ethanol [27].

2.1.2.1 5-(2-Fluoro-4-methoxybenzylidene)thiazolidine-2,4-dione (1)

Yield: 88%. MP: 215–220°C.

IR ν_{max} (cm^{-1}): 3450.65, 3367.71, 3080.32, 3007.02, 2843.07, 1728.22, 1708.93, 1668.43, 1616.35, 1593.20, 1573.91, 1506.41, 1436.97, 1388.75, 1342.46, 1313.52, 1294.24, 1269.16, 1251.80, 1190.08, 1161.15, 1093.64, 1028.06, 950.91, 871.82, 858.32, 825.53, 806.25, 756.10, 729.09, 713.66, 692.44, and 646.15.

^{1}H NMR (400 MHz, DMSO-d_6) δ (ppm): 3.80 (s, 3H), 6.38 (s, 1H), 6.86–6.89 (m, 1H), 7.68 (d, J = 9.6 Hz, 1H), 8.49 (s, 1H), 10.41, and 11.18 (2 s, 1H).

^{13}C NMR (100 MHz, DMSO-d_6) δ (ppm): 55.76 (CH_3), 101.61 (d, J = 25.0 Hz, CH), 110.79 (CH), 113.05 (d, J = 12.8 Hz, C), 116.12 (C), 127.85 (CH), 130.23 (d, J = 3.8 Hz, CH), 155.41 (C), 160.85 (d, J = 11.5 Hz, C), 165.23 (C), and 167.44 (C).

MS (FAB) m/z 254.11 $[M + H]^+$.

Anal. Calcd. for $C_{11}H_8FNO_3S$: C, 52.17; H, 3.18; and N, 5.53. Found: C, 52.15; H, 3.19; and N, 5.54.

2.1.2.2 5-(2-Fluoro-5-methoxybenzylidene)thiazolidine-2,4-dione (2)

Yield: 55%. MP: 235–240°C.

IR ν_{max} (cm^{-1}): 3466.08, 3045.60, 2945.30, 2835.36, 1728.22, 1666.50, 1593.20, 1496.76, 1463.97, 1419.61, 1382.96, 1323.17, 1282.66, 1211.30, 1099.43, 1031.92, 1012.63, 956.69, 877.61, 839.03, 804.32, 758.02, 711.73, 694.37, and 644.22.

^{1}H NMR (400 MHz, DMSO-d_6) δ (ppm): 3.80 (s, 3H), 6.38 (s, 1H), 6.88–6.92 (m, 1H), 7.12–7.17 (m, 2H), 10.66, and 11.18 (2 brs, 1H).

^{13}C NMR (100 MHz, DMSO-d_6) δ (ppm): 55.70 (CH_3), 113.73 (d, J = 1.9 Hz, CH), 115.78 (CH), 115.88 (d, J = 3.2 Hz, CH), 116.12 (C), 121.23 (d, J = 14.1 Hz, C), 129.86 (d, J = 1.9 Hz, CH), 155.53 (C), 160.79 (C), 165.13 (C), and 167.44 (C).

MS (FAB) m/z 254.14 $[M + H]^+$.

Anal. Calcd. for $C_{11}H_8FNO_3S$: C, 52.17; H, 3.18; and N, 5.53. Found: C, 52.19; H, 3.17; and N, 5.52.

2.1.2.3 5-(2-Hydroxy-3-methylbenzylidene)thiazolidine-2,4-dione (3)

Yield: 36%. MP: 168–170°C.

IR ν_{max} (cm^{-1}): 3541.31, 3431.36, 3336.85, 3050.46, 2924.09, 2858.51, 1693.50, 1681.93, 1600.92, 1525.69, 1469.76, 1435.04, 1381.03, 1265.30, 1188.15, 1095.57, 1039.63, 765.74, 746.45, 680.87, and 650.01.

^{1}H NMR (400 MHz, DMSO-d_6) δ (ppm): 2.30 (s, 3H), 6.66–7.44 (m, 3H), 8.50 (s, 1H), 10.12 (s, 1H), 10.41, and 11.18 (2 s, 1H).

^{13}C NMR (100 MHz, DMSO-d_6) δ (ppm): 15.23 (CH_3), 116.10 (C), 116.40 (C), 122.43 (CH), 125.82 (CH), 126.11 (C), 129.86 (CH), 131.20 (CH), 150.15 (C), 165.13 (C), and 167.44 (C).

MS (FAB) m/z 236.16 $[M + H]^+$.

Anal. Calcd. for $C_{11}H_9NO_3S$: C, 56.16; H, 3.86; and N, 5.95. Found: C, 56.13; H, 3.87; and N, 5.97.

2.1.2.4 5-(2-Hydroxy-5-methoxy-3-nitrobenzylidene) thiazolidine-2,4-dione (4)

Yield: 74%. MP: 245–246°C.

IR ν_{max} (cm^{-1}): 3562.52, 3425.58, 3334.92, 3076.46, 2945.30, 1693.50, 1681.93, 1668.43, 1598.99, 1537.27, 1531.48, 1454.33, 1344.38, 1307.74, 1242.16, 1197.79, 1166.93, 1095.57, 1041.56, 929.69, 837.11, 752.24, and 665.44.

^{1}H NMR (400 MHz, DMSO-d_6) δ (ppm): 3.81 (s, 3H), 6.72–6.88 (m, 1H), 7.87–8.02 (m, 1H), 8.47 (s, 1H), 10.26 (s, 1H), and 11.10 (brs, 1H).

^{13}C NMR (100 MHz, DMSO-d_6) δ (ppm): 55.78 (CH_3), 108.20 (CH), 116.06 (C), 118.01 (CH), 118.42 (C), 135.55 (CH), 137.90 (C), 145.44 (C), 155.05 (C), 165.30 (C), and 167.40 (C).

MS (FAB) m/z 297.14 $[M + H]^+$.

Anal. Calcd. for $C_{11}H_8N_2O_6S$: C, 44.60; H, 2.72; and N, 9.46. Found: C, 44.63; H, 2.71; and N, 9.44.

2.1.2.5 5-(3-Chloro-4-fluorobenzylidene)thiazolidine-2,4-dione (5)

Yield: 68%. MP: 218–224°C.

IR ν_{max} (cm^{-1}): 3444.87, 3387.00, 3037.89, 1737.86, 1708.93, 1668.43, 1591.27, 1504.48, 1435.04, 1346.31, 1263.37, 1195.87, 1126.43, 1091.71, 1060.85, 1024.20, 920.05, 898.83, 864.11, 819.75, 792.74, 756.10, 729.09, 709.80, 675.09, and 642.30.

^{1}H NMR (400 MHz, DMSO-d_6) δ (ppm): 6.37 (s, 1H), 7.39 (t, J = 8.8 Hz, 1H), 7.83 (d, J = 5.6 Hz, 1H), 8.49 (s, 1H), 10.67, and 11.25 (2 brs, 1H).

^{13}C NMR (100 MHz, DMSO-d_6) δ (ppm): 116.91 (C), 117.02 (d, J = 21.2 Hz, CH), 120.09 (d, J = 17.3 Hz, C), 128.70 (d, J = 1.9 Hz, CH), 130.15 (d, J = 7.0 Hz, CH), 130.72 (C), 130.96 (d, J = 3.8 Hz, CH), 155.38 (C), 165.27 (C), and 167.45 (C).

MS (FAB) m/z 258.06 $[M + H]^+$.

Anal. Calcd. for $C_{10}H_5ClFNO_2S$: C, 61.78; H, 4.75; and N, 6.00. Found: C, 61.81; H, 4.73; and N, 6.01.

2.1.2.6 5-(3-Chloro-4-methylbenzylidene)thiazolidine-2,4-dione (6)

Yield: 83%. MP: 225–230°C.

IR ν_{max} (cm^{-1}): 3456.44, 3375.43, 3028.24, 2929.87, 1728.22, 1710.86, 1660.71, 1589.34, 1496.76, 1440.83, 1392.61, 1361.74, 1334.74, 1284.59, 1253.73, 1219.01, 1188.15, 1124.50, 1087.85, 1053.13, 1031.92, 997.20, 906.54, 887.26, 860.25, 821.68, 756.10, 711.73, 675.09, 644.22, and 632.65.

^{1}H NMR (400 MHz, DMSO-d_6) δ (ppm): 2.32 (s, 3H), 6.35 (s, 1H), 7.33 (d, J = 8.0 Hz, 1H), 7.66 (s, 1H), 8.48 (s, 1H), 10.61, and 11.21 (2 brs, 1H).

^{13}C NMR (100 MHz, DMSO-d_6) δ (ppm): 19.35 (CH_3), 116.91 (C), 127.94 (CH), 128.29 (CH), 128.97 (CH), 131.29 (C), 132.52 (C), 133.80 (C), 135.55 (CH), 165.35 (C), and 167.45 (C).

MS (FAB) m/z 254.17 $[M + H]^+$.

Anal. Calcd. for $C_{11}H_8ClNO_2S$: C, 52.08; H, 3.18; and N, 5.52. Found: C, 52.05; H, 3.20; and N, 5.52.

2.1.2.7 5-(3-Methoxy-2-nitrobenzylidene)thiazolidine-2,4-dione (7)

Yield: 43%. MP: 190–195°C.

IR ν_{max} (cm^{-1}): 3323.35, 3022.45, 2941.44, 2837.29, 1658.78, 1651.07, 1598.99, 1537.27, 1454.33, 1402.25, 1359.82, 1261.45, 1178.51, 1118.71, 1068.56, 1039.63, 995.27, 852.54, 732.95, and 642.30.

^{1}H NMR (400 MHz, DMSO-d_6) δ (ppm): 3.83 (s, 3H), 6.85–7.90 (m, 3H), 8.69 (s, 1H), and 11.10 (brs, 1H).

^{13}C NMR (100 MHz, DMSO-d_6) δ (ppm): 55.76 (CH_3), 114.40 (CH), 116.50 (C), 119.69 (CH), 128.90 (C), 131.30 (C), 134.99 (CH), 136.56 (CH), 155.41 (C), 165.36 (C), and 167.47 (C).

MS (FAB) m/z 281.16 $[M + H]^+$.

Anal. Calcd. for $C_{11}H_8N_2O_5S$: C, 47.14; H, 2.88; and N, 10.00. Found: C, 47.11; H, 2.89; and N, 10.02.

2.1.2.8 5-(5-Chloro-2-hydroxy-3-methylbenzylidene) thiazolidine-2,4-dione (8)

Yield: 40%. MP: 160–165°C.

IR ν_{max} (cm^{-1}): 3541.31, 3454.51, 3334.92, 3076.46, 2927.94, 1693.50, 1681.93, 1598.99, 1566.20, 1514.12, 1469.76, 1435.04, 1381.03, 1311.59, 1192.01, 1120.64, 1043.49, 900.76, 864.11, 752.24, 731.02, 651.94, and 634.58.

^{1}H NMR (400 MHz, DMSO-d_6) δ (ppm): 2.26 (s, 3H), 6.92–7.68 (m, 2H), 8.51 (s, 1H), 10.21 (s, 1H), and 11.10 (brs, 1H).

^{13}C NMR (100 MHz, DMSO-d_6) δ (ppm): 15.25 (CH_3), 116.61 (C), 117.89 (C), 124.78 (CH), 126.76 (C), 129.39 (CH), 132.80 (C), 135.56 (CH), 150.15 (C), 165.31 (C), and 167.42 (C).

MS (FAB) m/z 270.12 $[M + H]^+$.

Anal. Calcd. for $C_{11}H_8ClNO_3S$: C, 48.99; H, 2.99; and N, 5.19. Found: C, 48.98; H, 2.97; and N, 5.21.

2.2 Biochemistry

2.2.1 AR activity assay

Purification of sheep liver AR was done according to the previous studies [28–32]. Bradford method was utilized to determine the quantitative protein [33]. The enzyme purity was checked according to Laemmli's procedure [34,35]. AR activity was spectrophotometrically evaluated based on the decrease in absorbance of NADPH at 340 nm [36–38].

2.2.2 *In vitro* inhibition studies

The AR activity was determined in the presence of different concentrations of compounds **1**–**8**. The IC_{50} value of each compound was calculated from activity%–[Compound] graphs [36]. For determining the inhibition types of the compounds, Lineweaver–Burk graph was plotted [39] according to the previous works [40–42].

2.2.3 Cell culture and drug treatment

The L929 mouse fibroblast cells (ATCC, CCL-1^{TM}) (Manassas, VA, USA) were cultured and drug treatments were performed as previously reported [42].

2.2.4 MTT assay

MTT test was performed to examine the cytotoxic effects of compounds **1**–**8** on the L929 cells as previously explained [43] but with minor modifications [42].

The percentage of the viable cells was calculated using the following formula: (%) = [100 × (sample absorbance)/(control absorbance)].

2.2.5 Statistical studies

GraphPad Prism version 7 for Mac (GraphPad Software, La Jolla, CA, USA) was used for data analysis and graphs. SigmaPlot version 12 for Windows (Systat Software, San Jose, CA, USA) was performed to calculate the inhibition constants. The fit of enzyme inhibition models was compared using the extra sum-of-squares F test and the Akaike's corrected Information Criterion (AICc) approach. The results were expressed as mean ± standard error of the

mean (95% confidence intervals). Differences between data sets were considered statistically significant when the p value was less than 0.05.

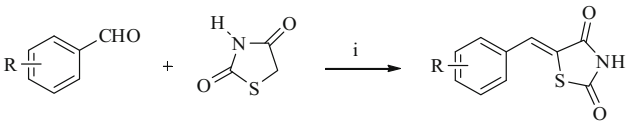

Scheme 1: The synthetic route for the preparation of compounds **1–8**. Reagents and conditions: (i) NH_2CONH_2, oil bath, 150°C, 2 h.

2.3 Molecular docking studies

Molecular docking simulations were conducted using panels (LigPrep [44], Maestro [45], Prime molecular mechanics–generalized Born surface area [MM-GBSA] [46], Protein Preparation Wizard [47], and Receptor Grid Generation [48]) in the Schrödinger Suite 2020-2 for Mac. The high-resolution 3D crystal structure of AR (PDB ID: 4JIR; 2.00 Å) [49] was downloaded from RCSB Protein Data Bank [50] and used for molecular docking. Protein Preparation Wizard [51] was used to prepare the crystal structure [52]. The 3D structures of compounds **1–8** were sketched using ChemDraw Pro version 19.1 for Mac [53] (PerkinElmer, Inc., Waltham, MA, USA). The molecules were subjected to ligand preparation using LigPrep tool [54] in default conditions at pH 7.4 ± 0.5 [55] with Epik [56] in the OPLS3e force field [57,58]. Receptor Grid Generation tool [59] was used to generate the grid for docking. Binding sites were defined using cocrystallized natural ligand (EPR). Glide extra precision (Glide XP) [60,61] was used for docking [62]. Docked poses were rescored using the MM-GBSA approach [63,64].

2.4 *In silico* ADME studies

QikProp, a predictive ADME module within the Maestro suite produced by Schrödinger, was performed to predict the ADME properties of compounds **1–8**.

Ethical approval: The conducted research is not related to either human or animal use.

3 Results and discussion

3.1 Chemistry

The preparation of the hitherto unreported 5-(arylidene) thiazolidine-2,4-diones (**1–8**) was carried out through the solvent-free reaction of 2,4-TZD with aromatic aldehydes in the presence of urea (Scheme 1).

The structures of compounds **1–8** were verified by IR, ^{1}H NMR, ^{13}C NMR, mass spectrometry and elemental analyses. In their IR spectra, the C=O stretching vibrations resulted in the formation of two characteristic bands at 1737.86–1651.07 cm^{-1}. The N–H stretching vibration belonging to the N–H proton of the thiazolidine scaffold gave rise to the bands in the region 3466.08–3323.35 cm^{-1}. In the IR spectra of compounds **3**, **4**, and **8**, the O–H stretching band appeared at 3562.52–3541.31 cm^{-1}. In the ^{1}H NMR spectra of all compounds except compound **2**, the signal due to the benzylidene CH proton was observed at 8.47–8.69 ppm as a singlet. In the ^{1}H NMR spectra of compounds **4**, **7**, and **8**, the signal due to the N–H proton appeared at 11.10 ppm as a broad singlet, whereas in the ^{1}H NMR spectra of other compounds, the signal due to the N–H proton appeared in the region 10.41–11.25 ppm as two singlets or broad singlets. In the ^{1}H NMR spectra of methoxy-substituted compounds **1**, **2**, **4**, and **7**, the signal due to the methoxy protons was observed in the region 3.80–3.83 ppm as a singlet. In the ^{1}H NMR spectra of methyl-substituted compounds **3**, **6**, and **8**, the signal due to the methyl protons occurred in the region 2.26–2.32 ppm as a singlet. The O–H proton gave rise to a singlet peak at 10.12–10.26 ppm in the ^{1}H NMR spectra of compounds **3**, **4**, and **8**. In the ^{13}C NMR spectra of compounds **1–8**, the signals due to the carbons of two C=O groups were observed in the region 165.13–167.47 ppm. The signal due to the benzylidene CH carbon appeared at 129.86–136.56 ppm. In the ^{13}C NMR spectra of methoxy-substituted compounds **1**, **2**, **4**, and **7**, the methoxy carbon gave rise to the peak at 55.70–55.78 ppm. In the ^{13}C NMR spectra of methyl-substituted compounds **3**, **6**, and **8**, the signal due to the methyl carbon occurred in the region 15.23–19.35 ppm.

3.2 *In vitro* AR inhibitory activity and cytotoxicity

The IC_{50}, K_i, and inhibition types of compounds **1–8** were determined to investigate their ability to inhibit AR (Table 1). According to *in vitro* data, compounds **1–8** showed inhibitory effects on AR, with IC_{50} values ranging from 0.273 to 0.533 μM and K_i values ranging from 0.445 to 0.943 μM (Figure 2). Compounds **1**, **3**, and **5** were found to act as uncompetitive AR inhibitors, whereas other

Table 1: AR inhibition data of compounds **1–8**

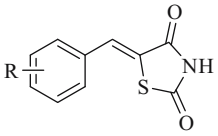

Compound	R	IC_{50} (μM)	R^2	K_i (μM)	R^2	Inhibition type
1	2-F-4-OCH_3	0.375 ± 0.007	0.9970	0.462 ± 0.015	0.9964	Uncompetitive
2	2-F-5-OCH_3	0.273 ± 0.004	0.9981	0.549 ± 0.023	0.9923	Non-competitive
3	2-OH-3-CH_3	0.382 ± 0.010	0.9955	0.445 ± 0.013	0.9982	Uncompetitive
4	2-OH-5-OCH_3-3-NO_2	0.349 ± 0.003	0.9994	0.769 ± 0.017	0.9977	Non-competitive
5	3-Cl-4-F	0.398 ± 0.011	0.9920	0.892 ± 0.020	0.9983	Uncompetitive
6	3-Cl-4-CH_3	0.411 ± 0.005	0.9991	0.729 ± 0.019	0.9957	Non-competitive
7	3-OCH_3-2-NO_2	0.455 ± 0.008	0.9963	0.713 ± 0.014	0.9976	Non-competitive
8	2-OH-3-CH_3-5-Cl	0.533 ± 0.015	0.9935	0.943 ± 0.024	0.9960	Non-competitive

The test results were indicated as mean ± standard deviation.

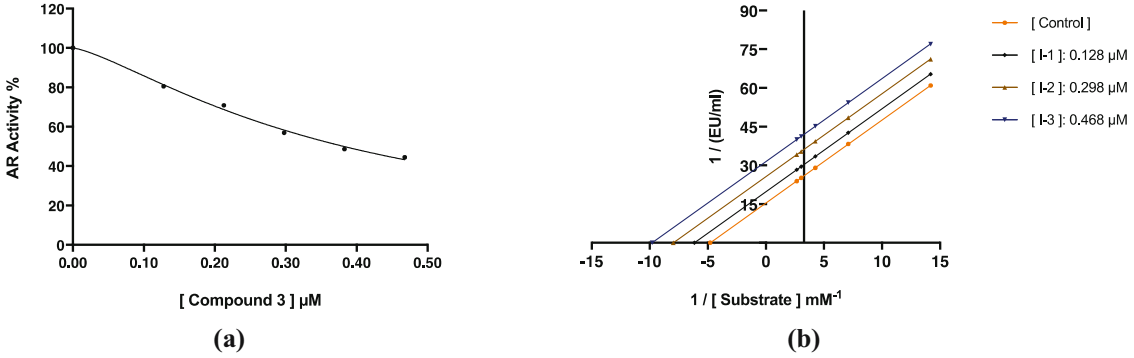

Figure 2: (a) Percentage activity versus inhibitor concentration graph of compound **3** at five different concentrations. (b) Lineweaver–Burk plot of compound **3**.

compounds were identified as noncompetitive AR inhibitors. The order of 2,4-TZD-based AR inhibitors (**1**–**8**) (from the most active to the least active) according to their K_i values was noted to be as follows: compound **3** > compound **1** > compound **2** > compound **7** > compound **6** > compound **4** > compound **5** > compound **8**. The *in vitro* data pointed out the significance of the arylidene group at the fifth position of 2,4-TZD scaffold. The introduction of a chlorine group into the fifth position of the benzylidene moiety of compound **3** (IC_{50} = 0.382 ± 0.010 μM, K_i = 0.445 ± 0.013 μM) led to a substantial decrease in AR inhibitory potency (IC_{50} = 0.533 ± 0.015 μM, K_i = 0.943 ± 0.024 μM for compound **8**) and an alteration in inhibition type (the inhibition type of compound **3** was uncompetitive, while the inhibition type of compound **8** was noncompetitive).

In the search for AR inhibitors for the management of T2D and its complications, the identification of potent therapeutic agents endowed with favorable pharmacokinetic profiles as well as devoid of severe unwanted effects is an uphill task for researchers [5]. On this basis, herein

Table 2: IC_{50} values of compounds **1–8** for L929 cell line after 24 h incubation

Compound	IC_{50} (μM)[a]
1	0.55 ± 0.07
2	2.63 ± 0.15
3	8.9 ± 0.66
4	2.25 ± 0.35
5	3.47 ± 0.84
6	1.43 ± 0.06
7	>25
8	>25

[a] Results were given as mean ± SD.

the cytotoxic activities of compounds **1**–**8** against L929 mouse fibroblast (healthy) cells were determined (Table 2). According to the MTT assay, all compounds did not show significant cytotoxicity toward L929 cells at their effective concentrations. The IC_{50} values of compounds **2**–**6** for L929 cells were found to be between 1.43 and 8.9 µM, while the IC_{50} values of compounds **7** and **8** for L929 cell line were higher than 25 µM, pointing out the safety of compounds **2**–**8** as AR inhibitors. However, the IC_{50} value of compound **1** for L929 cells (IC_{50} = 0.55 ± 0.07 µM) was slightly close to its IC_{50} value for AR inhibition (IC_{50} = 0.375 ± 0.007 µM). The effects of compound **1** on percentages of L929 cell viability at different concentrations (0.39, 0.78, and 6.26 µM) were found as 68.85 ± 2.47, 38.61 ± 14.71, and 31.60 ± 3.15, respectively ($p < 0.05$). These results showed that compound **1** caused dose-dependent cytotoxicity on L929 cell line at tested concentrations. On the other hand, the effects of compound **3**

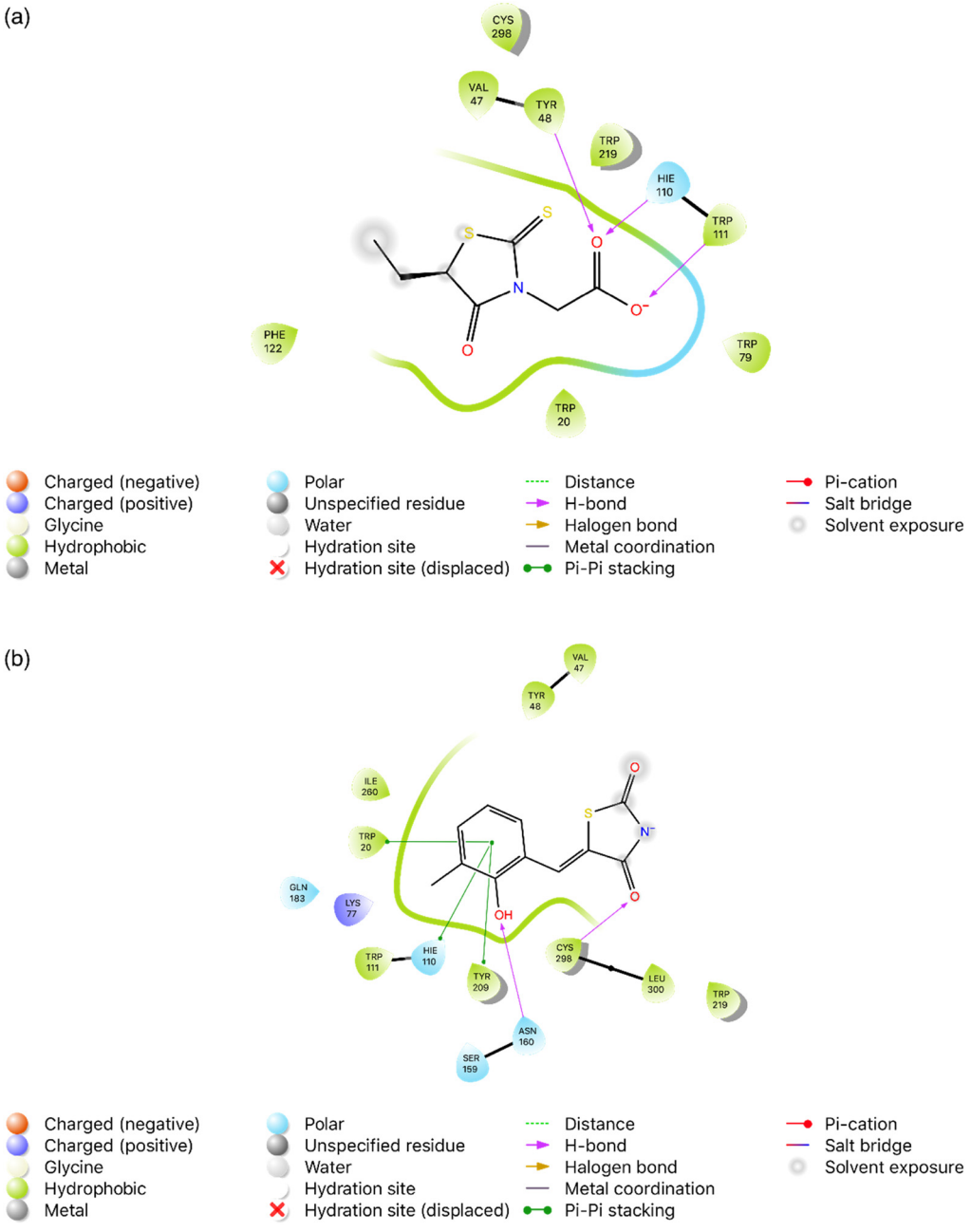

Figure 3: Interactions of the ligands with the key amino acids within the binding site of AR (PDB ID: 4JIR, 2.00 Å). (a) 2D ligand interaction diagram of 4JIR with native ligand EPR (epalrestat). (b) 2D ligand interaction diagram of 4JIR with compound **3**.

on percentages of L929 cell viability at different concentrations (0.78, 6.26, and 12.5 μM) were determined as 92.22 ± 5.43, 91.99 ± 13.69, and 22.72 ± 2.39, respectively ($p < 0.05$). The cytotoxicity of compound **3** was low at 0.78 and 6.26 μM. This outcome indicated that compound **3** displayed low cytotoxicity toward L929 cell line at its IC_{50} value for AR inhibition (IC_{50} = 0.382 ± 0.010 μM).

3.3 Molecular docking studies

In an effort to gain insight into the binding mode of the TZD scaffold in the enzyme binding site, compound **3** carrying 2-hydroxy-3-methylbenzylidene moiety at the fifth position of 2,4-TZD scaffold was docked into the binding site of AR (PDB ID: 4JIR) as a representative of compounds **1**–**8** (Figure 3). The best poses for ligand according to score and binding interactions were refined by the MM-GBSA-based approach to assess the electrostatic contribution of the variable dielectric surface generalized born (VSGB) solvation model. For validation of molecular docking simulations, the cocrystalized ligand EPR was extracted and redocked into the binding site. Their root mean square deviation (RMSD) score was computed to evaluate the quality of the cocrystallized ligand. The results were compared with EPR derived from the corresponding 4JIR, and the docking poses were superimposed. The RMSD score was found as 1.20 Å. The docking pattern of EPR was compared with that of compound **3**.

According to Zhang et al. [49], the native ligand EPR (with an MM-GBSA value of −33.42 kcal/mol and a docking score of −7.19) formed three H-bonds with Tyr48, His110, and Trp111 (with distances 1.56, 1.83, and 2.25 Å, respectively), in the catalytic domain of 4JIR. Moreover, the most prominent amino acid residues accommodating hydrophobic fragments were Tyr48 and Trp111 as well as Trp20, Val47, Trp79, Phe122, Trp219, and Cys298. Compound **3** (with an MM-GBSA value of −33.69 kcal/mol and a docking score of −7.19) exhibited two interactions with the target enzyme. Asn160 and Cys298 showed H-acceptor interactions with the hydroxyl and carbonyl groups (with distances 2.10 and 2.41 Å, respectively) of the ligand. The weak π–π stacking between Trp20, His110, and Tyr209 residues and the benzylidene moiety was observed in the 2D ligand interaction diagram (Figure 3). The results provided insights into the interactions between compounds **1**–**8** and AR and rationalized the experimental data.

3.4 *In silico* pharmacokinetic studies

The discovery of AR inhibitors with favorable ADME profiles represents a crucial turning point in the challenging route to develop a new generation of safer AR inhibitors [5]. On this basis, the pharmacokinetic features of compounds **1**–**8** were assessed by means of QikProp (Table 3). According to *in silico* prediction, their SASA, QPlogPo/w, CIQPlogS, and QPlogKhsa values were within the recommended

Table 3: Predicted ADME profiles of compounds **1**–**8**

Compound	SASA[a]	QPlogPo/w[a]	CIQPlogS[a]	QPlogKhsa[a]	Human oral absorption%[b]	Rule of five[c]	Rule of three[c]
1	428.912	1.786	−3.528	−0.236	86.866	0	0
2	421.221	1.746	−3.528	−0.240	86.630	0	0
3	423.671	1.156	−3.130	−0.293	77.063	0	0
4	465.209	0.375	−3.705	−0.406	56.281	0	0
5	417.076	2.184	−3.892	−0.145	89.199	0	0
6	436.250	2.144	−3.813	−0.044	88.965	0	0
7	456.458	1.058	−3.691	−0.304	70.607	0	0
8	448.637	1.694	−3.791	−0.188	81.474	0	0

[a] Recommended values for the total solvent accessible surface area (SASA): 300–1,000 $Å^2$; the predicted octanol/water partition coefficient (QPlogPo/w): −2 to 6.5; the conformation-independent predicted aqueous solubility (CIQPlogS): −6.5 to 0.5; the predicted binding to human serum albumin (QPlogKhsa): −1.5 to 1.5.[b] Predicted human oral absorption on 0 to 100% scale. Human oral absorption higher than 80% is considered to be high, while human oral absorption lower than 25% is considered to be poor.[c] Rule of Five: Number of violations of Lipinski's rule of five. The rules are molecular weight of the molecule < 500, QPlogPo/w < 5, hydrogen-bond donor atoms ≤5, hydrogen-bond acceptor atoms ≤ 10. Compounds that provide these rules are considered as drug-like molecules. Rule of Three: Number of violations of Jorgensen's rule of three. The three rules are QPlogS (predicted aqueous solubility) > −5.7, QPPCaco > 22 nm/s, # primary metabolites < 7. Compounds with fewer (and preferably no) violations of these rules are more likely to be orally available agents (Schrödinger Release 2016-2: Schrödinger, LLC, New York, NY, USA).

range. Their human oral absorption percentages were found to range from 56.281 to 89.199%. All compounds comply with Lipinski's rule of five and Jorgensen's rule of three, and therefore they are expected to have favorable oral bioavailability and drug-like features.

4 Conclusions

In conclusion, a facile and versatile synthetic procedure was performed to obtain new 5-(arylidene)thiazolidine-2,4-diones, which were evaluated for their AR inhibitory effects and cytotoxic effects on L929 cells. According to *in vitro* assay, compounds **1**–**8** showed inhibitory effects on AR with K_i values ranging from 0.445 to 0.943 μM. Taking into account the K_i values, compound **3** was found as the most promising AR inhibitor with a K_i value of 0.445 ± 0.013 μM and its inhibition type was determined as uncompetitive. The MTT assay indicated that compound **3** did not exert cytotoxicity toward L929 cells at its effective concentration. Based on molecular docking studies, compound **3** interacted with crucial amino acid residues in the binding site of AR (PDB ID: 4JIR). Taking into account *in silico* ADME studies, this compound is expected to have a favorable pharmacokinetic profile. *In vitro* and *in silico* studies pointed out the potential of compound **3** as an orally bioavailable AR inhibitor for the management of T2D complications as well as nondiabetic diseases.

Funding: This work was supported by the Research Fund of Anadolu University (grant numbers: 2005S019 and 1610S681), the Research Fund of Ardahan University (grant number: 2019-008), and the Research Fund of Erzincan Binali Yıldırım University (grant number: FBA-2017-501).

Author contributions: BS was involved in conceptualization, investigation, formal analysis, methodology, software, writing of the original draft, reviewing, and editing; MDA was in charge of conceptualization, data curation, formal analysis, funding acquisition, investigation, methodology, project administration, resources, software, writing – writing of the original draft, reviewing, and editing; YD contributed to data curation, formal analysis, funding acquisition, methodology, project administration, resources, software, validation, visualization, writing of the original draft, reviewing, and editing; CT was involved in data curation, formal analysis, funding acquisition, methodology, project administration, resources, software, validation, visualization, writing of the original draft, reviewing, and editing; KÖ contributed to investigation, methodology, writing, reviewing, and editing; GAÇ was in charge of data curation, formal analysis, methodology, software, validation, writing, reviewing, and editing; ŞB was involved in conceptualization, methodology, software, project administration, resources, writing, reviewing, and editing; AÖ contributed to conceptualization, methodology, software, resources, writing, reviewing, and editing.

Conflict of interest: Belgin Sever, the coauthor of this article, is a current Editorial Board member of Open Chemistry. This fact did not affect the peer-review process. The authors declare no other conflict of interest.

Data availability statement: All data generated or analyzed during this study are included in this published article [and its supplementary information files].

References

[1] Schäfer SA, Machicao F, Fritsche A, Häring H-U, Kantartzis K. New type 2 diabetes risk genes provide new insights in insulin secretion mechanisms. Diabetes Res Clin Pract. 2011;93:S9–24.
[2] Liu Y, Hu Y, Liu T. Recent advances in non-peptidomimetic dipeptidyl peptidase 4 inhibitors: medicinal chemistry and preclinical aspects. Curr Med Chem. 2012;19:3982–99.
[3] Kerru N, Singh-Pillay A, Awolade P, Singh P. Current anti-diabetic agents and their molecular targets: a review. Eur J Med Chem. 2018;152:436–88.
[4] De S, Banerjee S, Kumar SKA, Paira P. Critical role of dipeptidyl peptidase IV: a therapeutic target for diabetes and cancer. Mini Rev Med Chem. 2019;19:88–97.
[5] Maccari R, Ottanà R. Targeting aldose reductase for the treatment of diabetes complications and ınflammatory diseases: new insights and future directions. J Med Chem. 2015;58:2047–67.
[6] Costantino L, Rastelli G, Gamberini MC, Barlocco D. Pharmacological approaches to the treatment of diabetic complications. Exp Opin Ther Pat. 2000;10:1245–62.
[7] Brownlee M. Biochemistry and molecular cell biology of diabetic complications. Nature. 2001;414:813–20.
[8] Lorenzi M. The polyol pathway as a mechanism for diabetic retinopathy: attractive, elusive, and resilient. Exp Diabetes Res. 2007;2007:61038.
[9] Ramana KV. Aldose reductase: new insights for an old enzyme. BioMol Concepts. 2011;2:103–14.
[10] Grewal AS, Bhardwaj S, Pandita D, Lather V, Sekhon BS. Updates on aldose reductase inhibitors for management of diabetic complications and non-diabetic diseases. Mini Rev Med Chem. 2016;16:120–62.

[11] Sangshetti JN, Chouthe RS, Sakle NS, Gonjari I, Shinde DB. Aldose reductase: a multi-disease target. Curr Enzym Inhib. 2014;10:2–12.
[12] Quattrini L, La Motta C. Aldose reductase inhibitors: 2013-present. Expert Opin Ther Pat. 2019;29:199–213.
[13] Dowarah J, Singh VP. Anti-diabetic drugs recent approaches and advancements. Bioorg Med Chem. 2020;28:115263.
[14] Jain AK, Vaidya A, Ravichandran V, Kashaw SK, Agrawal RK. Recent developments and biological activities of thiazolidinone derivatives: a review. Bioorg Med Chem. 2012;20:3378–95.
[15] Jain VS, Vora DK, Ramaa CS. Thiazolidine-2,4-diones: Progress towards multifarious applications. Bioorg Med Chem. 2013;21:1599–620.
[16] Chadha N, Bahia MS, Kaur M, Silakari O. Thiazolidine-2,4-dione derivatives: programmed chemical weapons for key protein targets of various pathological conditions. Bioorg Med Chem. 2015;23:2953–74.
[17] Naim MJ, Alam MJ, Ahmad S, Nawaz F, Shrivastava N, Sahu M, et al. Therapeutic journey of 2,4-thiazolidinediones as a versatile scaffold: an insight into structure activity relationship. Eur J Med Chem. 2017;129:218–50.
[18] Kaur Manjal S, Kaur R, Bhatia R, Kumar K, Singh V, Shankar R, et al. Synthetic and medicinal perspective of thiazolidinones: a review. Bioorg Chem. 2017;75:406–23.
[19] Verma SK, Yadav YS, Thareja S. 2,4-Thiazolidinediones as PTP 1B inhibitors: a mini review (2012–2018). Mini Rev Med Chem. 2019;19:591–8.
[20] Bansal G, Thanikachalam PV, Maurya RK, Chawla P, Ramamurthy S. An overview on medicinal perspective of thiazolidine-2,4-dione: a remarkable scaffold in the treatment of type 2 diabetes. J Adv Res. 2020;23:163–205.
[21] Bruno G, Costantino L, Curinga C, Maccari R, Monforte F, Nicolò F, et al. Synthesis and aldose reductase inhibitory activity of 5-arylidene-2,4-thiazolidinediones. Bioorg Med Chem. 2002;10:1077–84.
[22] Maccari R, Del Corso A, Giglio M, Moschini R, Mura U, Ottanà R. *In vitro* evaluation of 5-arylidene-2-thioxo-4-thiazolidinones active as aldose reductase inhibitors. Bioorg Med Chem Lett. 2011;21:200–3.
[23] Maccari R, Vitale RM, Ottanà R, Rocchiccioli M, Marrazzo A, Cardile V, et al. Structure–activity relationships and molecular modelling of new 5-arylidene-4-thiazolidinone derivatives as aldose reductase inhibitors and potential anti-inflammatory agents. Eur J Med Chem. 2014;81:1–14.
[24] Chadha N, Silakari O. Identification of low micromolar dual inhibitors for aldose reductase (ALR2) and poly (ADP-ribose) polymerase (PARP-1) using structure based design approach. Bioorg Med Chem Lett. 2017;27:2324.
[25] Maccari R, Del Corso A, Paoli P, Adornato I, Lori G, Balestri F, et al. An investigation on 4-thiazolidinone derivatives as dual inhibitors of aldose reductase and protein tyrosine phosphatase 1B, in the search for potential agents for the treatment of type 2 diabetes mellitus and its complications. Bioorg Med Chem Lett. 2018;28:3712–20.
[26] Kousaxidis A, Petrou A, Lavrentaki V, Fesatidou M, Nicolaou I, Geronikaki A. Aldose reductase and protein tyrosine phosphatase 1B inhibitors as a promising therapeutic approach for diabetes mellitus. Eur J Med Chem. 2020;207:112742.
[27] Shah S, Singh B. Urea/thiourea catalyzed, solvent-free synthesis of 5-arylidenethiazolidine-2,4-diones and 5-arylidene-2-thioxothiazolidin-4-ones. Bioorg Med Chem Lett. 2012;22:5388–91.
[28] Aslan HE, Beydemir Ş. Phenolic compounds: the inhibition effect on polyol pathway enzymes. Chem Biol Interact. 2017;266:47.
[29] Demir Y, Duran HE, Durmaz L, Taslimi P, Beydemir Ş, Gulçin İ. The influence of some nonsteroidal anti-inflammatory drugs on metabolic enzymes of aldose reductase, sorbitol dehydrogenase, and α-glycosidase: a perspective for metabolic disorders. Appl Biochem Biotechnol. 2020;190:437–47.
[30] Demir Y, Işık M, Gülçin İ, Beydemir Ş. Phenolic compounds inhibit the aldose reductase enzyme from the sheep kidney. J Biochem Mol Toxicol. 2017;31:e21936.
[31] Şengül B, Beydemir Ş. The interactions of cephalosporins on polyol pathway enzymes from sheep kidney. Arch Physiol Biochem. 2018;124:35–44.
[32] Demir Y, Durmaz L, Taslimi P, Gulçin İ. Antidiabetic properties of dietary phenolic compounds: inhibition effects on α-amylase, aldose reductase, and α-glycosidase. Biotechnol Appl Biochem. 2019;66:781–6.
[33] Bradford MM. A rapid and sensitive method for the quantitation of microgram quantities of protein utilizing the principle of protein-dye binding. Anal Biochem. 1976;72:248–54.
[34] Laemmli UK. Cleavage of structural proteins during the assembly of the head of bacteriophage T4. Nature. 1970;227:680–5.
[35] Demir Y, Köksal Z. Some sulfonamides as aldose reductase inhibitors: Therapeutic approach in diabetes. Arch Physiol Biochem. 2020. doi: 10.1080/13813455.2020.1742166. in press.
[36] Cerelli MJ, Curtis DL, Dunn JP, Nelson PH, Peak TM, Waterbury LD. Antiinflammatory and aldose reductase inhibitory activity of some tricyclic arylacetic acids. J Med Chem. 1986;29:2347–51.
[37] Türkeş C, Demir Y, Beydemir Ş. Anti-diabetic properties of calcium channel blockers: inhibition effects on aldose reductase enzyme activity. Appl Biochem Biotechnol. 2019;189:318–29.
[38] Sever B, Altıntop MD, Demir Y, Akalın Çiftçi G, Beydemir Ş, Özdemir A. Design, synthesis, *in vitro* and *in silico* investigation of aldose reductase inhibitory effects of new thiazole-based compounds. Bioorg Chem. 2020;102:104110.
[39] Lineweaver H, Burk D. The determination of enzyme dissociation constants. J Am Chem Soc. 1934;56:658–66.
[40] Türkeş C, Söyüt H, Beydemir Ş. Effect of calcium channel blockers on paraoxonase-1 (PON1) activity and oxidative stress. Pharmacol Rep. 2014;66:74–80.
[41] Demir Y. The behaviour of some antihypertension drugs on human serum paraoxonase-1: an important protector enzyme against atherosclerosis. J Pharm Pharmacol. 2019;71:1576–83.
[42] Sever B, Altıntop MD, Demir Y, Pekdoğan M, Akalın Çiftçi G, Beydemir Ş, et al. An extensive research on aldose reductase inhibitory effects of new 4*H*-1,2,4-triazole derivatives. J Mol Struct. 2021;1224:129446.
[43] Mosmann T. Rapid colorimetric assay for cellular growth and survival: application to proliferation and cytotoxicity assays. J Immunol Methods. 1983;65:55–63.

[44] Türkeş C. Investigation of potential paraoxonase-I inhibitors by kinetic and molecular docking studies: chemotherapeutic drugs. Protein Pept Lett. 2019;26:392–402.
[45] Demir Y, Türkeş C, Beydemir Ş. Molecular docking studies and inhibition properties of some antineoplastic agents against paraoxonase-I. Anti-cancer Agents Med Chem. 2020;20:887–96.
[46] Işık M, Beydemir Ş, Demir Y, Durgun M, Türkeş C, Nasır A, et al. Benzenesulfonamide derivatives containing imine and amine groups: inhibition on human paraoxonase and molecular docking studies. Int J Biol Macromol. 2020;146:1111–23.
[47] Beydemir Ş, Türkeş C, Yalçın A. Gadolinium-based contrast agents: *In vitro* paraoxonase 1 inhibition, *in silico* studies. Drug Chem Toxicol. 2019. doi: 10.1080/01480545.2019.1620266. in press.
[48] Türkeş C. A potential risk factor for paraoxonase 1: *in silico* and *in vitro* analysis of the biological activity of proton-pump inhibitors. J Pharm Pharmacol. 2019;71:1553–64.
[49] Zhang L, Zhang H, Zhao Y, Li Z, Chen S, Zhai J, et al. Inhibitor selectivity between aldo–keto reductase superfamily members AKR1B10 and AKR1B1: Role of Trp112 (Trp111). FEBS Lett. 2013;587:3681–6.
[50] Işık M, Demir Y, Durgun M, Türkeş C, Necip A, Beydemir Ş. Molecular docking and investigation of 4-(benzylideneamino)- and 4-(benzylamino)-benzenesulfonamide derivatives as potent AChE inhibitors. Chem Pap. 2020;74:1395–405.
[51] Türkeş C, Beydemir Ş. Küfrevioğlu Öİ. *In vitro* and *in silico* studies on the toxic effects of antibacterial drugs as human serum paraoxonase 1 inhibitor. ChemistrySelect. 2019;4:9731–6.
[52] Türkeş C. Inhibition effects of phenolic compounds on human serum paraoxonase-1 enzyme. J Inst Sci Technol. 2019;9:1013–22.
[53] Durgun M, Türkeş C, Işık M, Demir Y, Saklı A, Kuru A, et al. characterisation, biological evaluation and *in silico* studies of sulphonamide Schiff bases. J Enzyme Inhib Med Chem. 2020;35:950–62.
[54] Türkeş C, Arslan M, Demir Y, Cocaj L, Nixha AR, Beydemir Ş. Synthesis, biological evaluation and *in silico* studies of novel *N*-substituted phthalazine sulfonamide compounds as potent carbonic anhydrase and acetylcholinesterase inhibitors. Bioorg Chem. 2019;89:103004.
[55] Işık M, Akocak S, Lolak N, Taslimi P, Türkeş C, Gülçin İ, et al. Synthesis, characterization, biological evaluation, and *in silico* studies of novel 1,3-diaryltriazene-substituted sulfathiazole derivatives. Arch Pharm. 2020;353:e2000102.
[56] Taslimi P, Işık M, Türkan F, Durgun M, Türkeş C, Gülçin İ, et al. Benzenesulfonamide derivatives as potent acetylcholinesterase, α-glycosidase, and glutathione S-transferase inhibitors: biological evaluation and molecular docking studies. J Biomol Struct Dyn. 2020. doi: 10.1080/07391102.2020.1790422. in press.
[57] Türkeş C, Demir Y, Beydemir Ş. Some calcium-channel blockers: kinetic and *in silico* studies on paraoxonase-I. J Biomol Struct Dyn. 2020. doi: 10.1080/07391102.2020.1806927. in press.
[58] Gündoğdu S, Türkeş C, Arslan M, Demir Y, Beydemir Ş. New isoindole-1,3-dione substituted sulfonamides as potent inhibitors of carbonic anhydrase and acetylcholinesterase: Design, synthesis, and biological evaluation. ChemistrySelect. 2019;4:13347–55.
[59] Türkeş C, Demir Y, Beydemir Ş. Calcium channel blockers: Molecular docking and inhibition studies on carbonic anhydrase I and II isoenzymes. J Biomol Struct Dyn. 2020. doi: 10.1080/07391102.2020.1736631. in press.
[60] Lolak N, Akocak S, Türkeş C, Taslimi P, Işık M, Beydemir Ş, et al. Synthesis, characterization, inhibition effects, and molecular docking studies as acetylcholinesterase, α-glycosidase, and carbonic anhydrase inhibitors of novel benzenesulfonamides incorporating 1,3,5-triazine structural motifs. Bioorg Chem. 2020;100:103897.
[61] Kılıç A, Beyazsakal L, Işık M, Türkeş C, Necip A, Takım K, et al. Mannich reaction derived novel boron complexes with amine-bis(phenolate) ligands: synthesis, spectroscopy and *in vitro*/*in silico* biological studies. J Organomet Chem. 2020;927:121542.
[62] Türkeş C, Beydemir Ş. Inhibition of human serum paraoxonase-I with antimycotic drugs: *in vitro* and *in silico* studies. Appl Biochem Biotechnol. 2020;190:252–69.
[63] Istrefi Q, Türkeş C, Arslan M, Demir Y, Nixha AR, Beydemir Ş, et al. Sulfonamides incorporating ketene *N*,*S*-acetal bioisosteres as potent carbonic anhydrase and acetylcholinesterase inhibitors. Arch Pharm. 2020;353:e1900383.
[64] Sever B, Türkeş C, Altıntop MD, Demir Y, Beydemir Ş. Thiazolylpyrazoline derivatives: *in vitro* and *in silico* evaluation as potential acetylcholinesterase and carbonic anhydrase inhibitors. Int J Biol Macromol. 2020;163:1970–88.